




Viral mimetic triggers cerebral arteriopathy in juvenile brain via neutrophil elastase and NETosis

Aditya Rayasam¹, Amandine Jullienne², Tetyana Chumak³, Joel Faustino¹, Jenny Szu², Mary Hamer², C Joakim Ek³, Carina Mallard³, Andre Obenaus² and Zinaida S Vexler¹ 

Abstract

Stroke is among the top ten causes of death in children but has received disproportionately little attention. Cerebral arteriopathies account for up to 80% of childhood arterial ischemic stroke (CAIS) cases and are strongly predictive of CAIS recurrence and poorer outcomes. The underlying mechanisms of sensitization of neurovasculature by viral infection are undefined. In the first age-appropriate model for childhood arteriopathy—by administration of viral mimetic TLR3-agonist Polyinosinic:polycytidylic acid (Poly-IC) in juvenile mice—we identified a key role of the TLR3-neutrophil axis in disrupting the structural-functional integrity of the blood-brain barrier (BBB) and distorting the developing neurovascular architecture and vascular networks. First, using an array of *in-vivo/post-vivo* vascular imaging, genetic, enzymatic and pharmacological approaches, we report marked Poly-IC-mediated extravascular leakage of albumin (66kDa) and of a small molecule Dil (~934Da) and disrupted tight junctions. Poly-IC also enhanced the neuroinflammatory milieu, promoted neutrophil recruitment, profoundly upregulated neutrophil elastase (NE), and induced neutrophil extracellular trap formation (NETosis). Finally, we show that functional BBB disturbances, NETosis and neuroinflammation are markedly attenuated by pharmacological inhibition of NE (Sivelestat). Altogether, these data reveal NE/NETosis as a novel therapeutic target for viral-induced cerebral arteriopathies in children.

Keywords

Neutrophil elastase, toll-like receptor 3, blood-brain barrier, sivelestat, neutrophil extracellular traps

Received 15 January 2021; Revised 11 June 2021; Accepted 13 June 2021

Introduction

Cerebral arteriopathies are a major risk factor for childhood arterial ischemic stroke (CAIS) and are strongly predictive of CAIS recurrence and poorer outcomes in children.^{1–3} Up to 80% of CAIS cases are attributed to arteriopathies,² yet the mechanistic understanding for how these vascular abnormalities develop in children is sparse in part due to the lack of appropriate models. Concepts have emerged relating to how the developmental stage of the brain plays a role in the pathophysiology of stroke in neonates, children and adults⁴ and how immune cells contribute to maturation-dependent vascular damage and brain injury.^{5–7} Findings in transient middle cerebral artery occlusion (tMCAO) models in neonatal and juvenile mice have demonstrated higher levels of albumin

leakage in juvenile compared to neonatal mice,⁶ underscoring the importance of age-appropriate models to mimic childhood disease and enhance the probability of translational success.

¹Department of Neurology, University California San Francisco, San Francisco, CA, USA

²Department of Pediatrics, University of California Irvine, Irvine, CA, USA

³Department of Physiology, Sahlgrenska Academy, University of Gothenburg, Gothenburg, Sweden

Corresponding author:

Zinaida S. Vexler, Department of Neurology, University California San Francisco, 675 Nelson Rising Lane, San Francisco, CA 94158, USA.
Email: Zena.Vexler@ucsf.edu

While the mechanisms of childhood arteriopathy onset and progression remain largely unknown, viral infections in children sensitize the cerebral vasculature, in part via immune mechanisms.^{8,9} Infections activate different subsets of leukocytes to inflame vessels, contribute to vessel fragility and increase susceptibility of children to stroke. Identifying which immune cells and which mechanisms contribute to viral infection-induced vascular disturbances will provide clues to develop therapies for arteriopathies and CAIS. Polyinosinic:polycytidylic acid (Poly-IC) is a viral mimetic and TLR3 agonist, which can both directly induce an inflammatory response in endothelial cells¹⁰ and indirectly disrupt endothelial properties by neutrophil signaling in sites of inflammation within vascular networks.^{11,12} Furthermore, Poly-IC can impair learning and memory in the developing brain¹³ and increase vulnerability to ischemic brain injury,¹⁴ suggesting that Poly-IC administration in juvenile rodents is appropriate to mimic vascular distortions, simulate childhood arteriopathies, and assess the impact of these vascular pathologies in relation to CAIS.

In adult stroke models, there is ample evidence of the damaging role of neutrophils early after injury.^{15–19} In humans, neutrophil accumulation is rapid and neurological outcomes are worse in patients with more severe neutrophil accumulation,^{20,21} but therapies targeting classic mechanisms of neutrophil activation have been largely ineffective for treating stroke.^{22,23} More recent adult stroke studies have identified disproportional activation of neutrophil extracellular traps (NETosis) as a potential major contributing factor affecting the magnitude of ischemic brain damage.^{24,25}

In a novel model of TLR3-induced viral infection that we developed in postnatal day 18 (P18) mice, we demonstrate robust vascular leakage, accumulation of peripheral leukocytes, activation of neutrophil elastase (NE) and triggered NETosis, which cumulatively lead to vasculopathy and sustained disruption of neurovascular networks in the maturing brain. Furthermore, we demonstrate that inhibition of NE proteolytic activity significantly limits neuroinflammation, Poly-IC-induced neurovascular leakages and longer-term neurovascular distortions. These findings reveal a novel potential therapeutic approach to prevent childhood arteriopathies and mitigate the susceptibility of the juvenile brain to CAIS.

Methods

Animals. All research conducted on animals was approved by the University of California San Francisco and University of California Irvine Institutional Animal Care and Use Committees and the Gothenburg Animal Ethics Committee (663/2018)

and in accordance to Guide for the Care and Use of Laboratory Animals (U.S. Department of Health and Human Services). Animals were given ad libitum access to food and water, housed with nesting material and shelters, and kept in rooms with temperature control and light/dark cycles. The data are in compliance with the ARRIVE 2.0 (Animal Research: Reporting *in vivo* experiments).²⁶ Wild type (WT) C57Bl/6 mice were bred internally. Heterozygous LysM-EGFP-ki mice on C57Bl/6 background were obtained from University of Missouri Mutant Mouse Regional Resource Center and bred at University of Gothenburg.

Polyinosinic:polycytidylic acid (Poly-IC) (5mg/kg, 2.5ul/gram body weight; Invivogen, San Diego, CA) or PBS was administered intraperitoneally (i.p.) to P18 C57BL/6 mice or LysM-EGFP-ki mice of both sexes. The timeline of outcomes is shown in Figure 1(a).

Albumin-647 conjugated bovine serum albumin (albumin^{Alexa-647}, Invitrogen) was injected retro-orbitally (5mg/kg, 1h before sacrifice, followed by transcardial PBS and ice-cold 4% PFA/PBS perfusion).^{5,6}

Nissl and immunofluorescence were accomplished in six sections from PBS-perfused or non-perfused, fixed, cryoprotected and flash frozen WT brains coronally sectioned on a cryostat (12um thick serial sections, 360um apart) as described.^{6,27} Slides were co-immunolabeled with rabbit anti-mouse Glut1 (1:500, Abcam), rat anti-mouse Ly6G (RB6-8C5; 1:200, Abcam), NE (1:500, Abcam) and H3cit (1:500 Abcam) and Z-stacks of images were captured (10–12 images, 1um step, 25× oil objective, Zeiss Axiovert 100 equipped with Volocity Software, Improvion/Perkin Elmer).^{6,27} Details for conditions and antibodies used are provided in the Supplemental Table 1. For non-perfused mice, antigen retrieval was performed. Glut1+/albumin^{Alexa-647} vessel coverage and extravascular albumin^{Alexa-647} were analyzed in 4–5 fields of view (FOV)/hemisphere/region in the cortex using automated protocols for signal intensity (SI) in a $1 \times 10^6 \mu\text{m}^3$ voxel and masks created using $\sim 2\text{SD}$ SI threshold from the Mean Fluorescence Intensity (MFI) of albumin^{Alexa-647} SI in the vessels. Background SI (lowest SI within the same FOV in each individual image) was subtracted.

GFP+Ly6G+ cells were quantified in Z-stacks (1.0um step size, 63× oil objective, or 2.0um step size, 20× air objective; Zeiss LSM800 Airyscan microscope) captured in multiple regions in two sections per LysM-EGFP-ki mouse (Olympus BX60, 40× air objective) co-stained with goat anti-CD31 (1:250, R&D systems), rat anti-mouse Ly6G (RB6-8C5; 1:200, Abcam) and rabbit anti-GFP (A-21311, 1:100, Invitrogen)

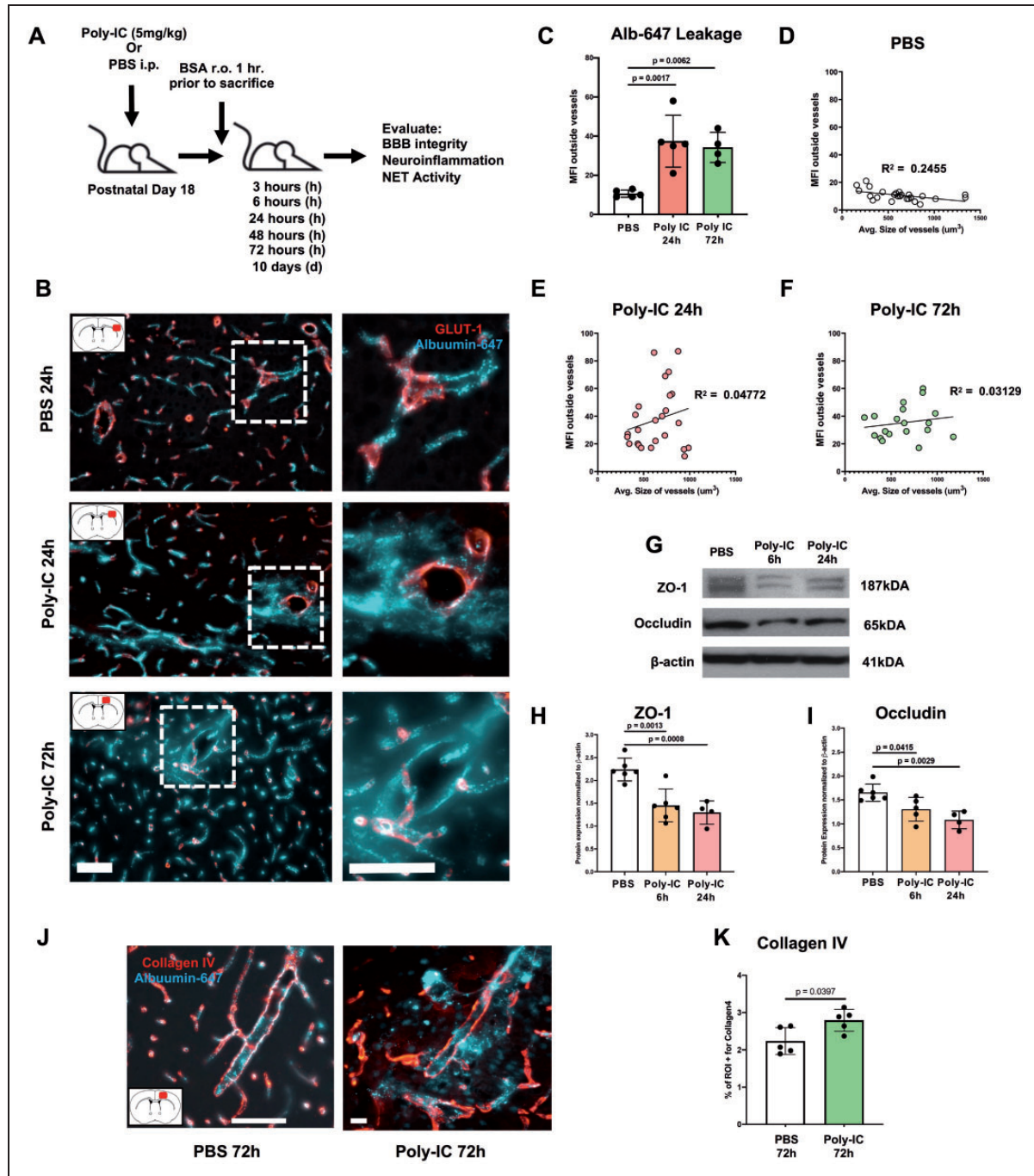


Figure 1. Viral mimetic Poly-IC triggers albumin leakage, adversely affects tight junction (TJ) proteins and increases vessel rigidity. (A) Experimental design to test Poly-IC effects in juvenile P18 mice. (B) Representative images of Albumin^{Alexa-647} (Alb-647) leakage (cyan) from vessels (Glut-1, red) into the cortical parenchyma after PBS injection (top), 24h (middle) and 72h (bottom) after Poly-IC injection. Scale bar = 80 um. Red rectangle in brain diagram depicts area where image was taken. Leakage was quantified in each group as Mean Fluorescence Intensity (MFI) outside of vessels and MFI outside vessels plotted versus average vessel size following PBS (C and D; $R^2 = 0.2455$, slope = -0.01087 to -0.001510 , RMSE = 3.354), 24h (C and E; $R^2 = 0.04772$, slope = 0.02327 , RMSE = 21.70) and 72h (C and F; $R^2 = 0.03129$, slope = 0.007934 , RMSE = 11.57) after Poly-IC administration. Representative Western blots (G) and quantification of ZO-1 (H) and occludin (I) 6h and 24h after Poly-IC/PBS administration. The data were normalized to β -actin expression. Representative images of Alb-647 with Collagen IV (red) in the cortex 72h after PBS (left) or Poly-IC injection (right) (J). Scale bar = 80 um. Quantification of %ROI+ for Collagen IV in the cortex 72h after PBS and Poly-IC (K). One-way ANOVA with post-hoc Bonferroni (normal distribution) or Kruskal-Wallis test (non-normal distribution) was performed to compare the variance in groups with one independent variable followed by Dunn post-hoc test (C, H, and I). Pearson's r correlation was utilized for (D-F). Student's t test with Mann-Whitney U test was performed for K. Individual p values are listed within figures for data that are significant.

antibodies. Images were processed using ImageJ software (version 1.53a).

Imaging and analysis of vascular painting (VP) was performed as previously described.⁶ Mice were i.p. injected with sodium nitroprusside (75 mg/kg) and heparin (20 mg/kg) 5 min before an i.p. injection of ketamine/xylazine (90/10 mg/kg). Cardiac injection of dye 1,1'-dioctadecyl-3,3,3'-tetramethylindo-carbocyanine perchlorate (DiI), 250 μ l pup <10 g; 375 μ l pup >10 g, 0.3 mg/ml of DiI in PBS 4% dextrose, was followed by perfusion fixation. Well-labeled brains were imaged axially using a fluorescent microscope (Keyence BZ-X810, Keyence). The right MCA vessels were imaged using a confocal microscope (10x, Olympus FV3000, Olympus Scientific). Images were analyzed for vessel density and length, number of junctions and lacunarity using the Angiotool software. Outliers using Grubbs' test were removed from final analysis.²⁸

Myeloid cell isolation and flow cytometry were performed on single cells from transcardially perfused mice following red blood cells lysis (ACK lysis buffer), centrifugation in 70%/30% Percoll gradient (1,220 g \times 30 min at 4°C without brake), and incubated with blocking buffer containing CD16/32 (1:100, Biolegend) in FACS staining buffer containing 2% FBS. Cells stained with anti-CD45-Pacific Blue, anti-CD11b-APC-Cy7, Ly6g (IA8)-AF700, Ly6c (Hk1.4)-APC, CXCR2-PE-Cy7, CCR2-PE (1:200; all from Biolegend) were measured on BD LSR II flow cytometer (BD Biosciences). Compensation beads and Fluorescence Minus One (FMO) samples, a commonly used strategy to prevent false positive results through overlap of fluorophores,²⁹ were applied. Gating and data analysis were performed using FlowJo software (Tree Star).

Western blot analysis was performed in cortical lysates using anti-occludin (1:500 AbCAM), ZO-1 (1:1000 AbCAM), NE (1:500 AbCAM), H3cit (1:500 AbCAM) and β -actin (1:5000 Sigma Aldrich), antibodies diluted in 5% milk in 0.2% Tween 20/TBS, 4°C, overnight.⁵

Multiplex cytokine assay was performed in cortex, plasma and CSF of transcardially saline-perfused mice using 23-plex cytokine kit (#M60009RDPD, Biorad), principally as we previously reported.^{6,27}

Neutrophil Elastase (NE) activity was determined by a kinetic assay in lysates from snap-frozen saline-perfused brains using a fluorogenic substrate (AbCAM ab204730) based on manufacturer's protocol. The fluorescent arbitrary units were read every 2 min for 1h (380 nmex/460 nmem), data acquired as relative fluorescent units (RFU)/min and normalized to protein concentration.

NE inhibitor sivelestat (SIV; 30 mg/kg, 20% DMSO in PBS, 2.5 μ l/g body weight; Tocris (Minneapolis, MS)

or vehicle (VEH; 20% DMSO in PBS) was administered i.p. into C57Bl/6 WT mice of both sexes twice daily starting at the time of Poly-IC injection.

Statistical analysis. Block litter design was used, mice of both sexes were randomized and analysis performed in blinded manner. Data distribution was tested for normality with Shapiro-Wilk test. Equality of variances was tested with Levine test. Two-way ANOVA with post-hoc Tukey's Multiple Comparison test was performed to compare groups with multiple independent variables. One-way ANOVA with post-hoc Bonferroni (normal distribution) or Kruskal-Wallis test (non-normal distribution) was performed to compare the variance in groups with one independent variable followed by Dunn post-hoc test. Student's t test with Mann-Whitney U test was performed to compare groups non-normal distribution. Pearson's r correlation was utilized for Figure 1. Two-way ANOVA with Sidak post-hoc analysis was performed to compare treatment versus time and treatment versus sex. GraphPad Prism 8 software (GraphPad) was utilized for statistical analysis and Grubbs' was used for outliers. Each dot on all graphs represents individual mouse. Individual p values are listed within figures for data that are significant. Results are shown as mean \pm SD.

Results

Viral mimetic Poly-IC triggers albumin leakage, adversely affects the tight junction (TJ) proteins and increases vessel rigidity

We first examined whether viral TLR3-mediated infection adversely affects growth of both male and female juvenile mice. By 72 h, while Poly-IC injected mice gained weight, the gain was significantly lower than in PBS treated mice and, further, was significantly lower in males compared to females administered with Poly-IC (Supplementary Figure 1). Next, we evaluated the magnitude of extravascular albumin leakage in the cortex of PBS and Poly-IC-treated mice using previously validated experimental protocol.^{5,6} Experimental design is shown in Figure 1A. In PBS-treated mice, albumin^{Alexa-647} injected 1h before sacrifice was retained intravascular, within Glut-1+ vessels (Figure 1B and C). In contrast, extravascular albumin^{Alexa-647} leakage into brain parenchyma was significantly increased in Poly-IC treated mice at both 24 and 72h (Figure 1B and C). To obtain insight of relationship between the magnitude of leakage and vessel size, we plotted MFI outside vessels against average size of vessels in the same regions and performed regression analysis (Figure 1D to F). Assessment of the

strength of the correlations between leakage and vessel size demonstrated lack of a relationship between leakage and vessel size in Poly-IC-treated mice at 24h and at 72h (Figure 1E and F).

Examination of whether albumin leakage through the blood-brain barrier (BBB) is associated with changes in expression of occludin and zonula occludens-1 (ZO-1), proteins localized at the TJ that reinforce and stabilize the BBB, showed that compared to PBS-treated mice, expression levels of ZO-1 (Figure 1G and H) and Occludin (Figure 1G and I) were significantly decreased as early as 6h after Poly-IC and remained low at 24h. Poly-IC also significantly increased vascular rigidity as was evident from increased collagen IV (Col IV) coverage of vessels 72h after treatment (Figure 1J and K). Thickening of Col IV coverage occurred regardless of vessel leakiness. Cumulatively, these results signify rapid Poly-IC-induced leakage through the paracellular route and functional-structural derangement at the neurovascular interface.

Poly-IC alters vessel architecture and adversely affects development of cortical vascular networks in juvenile mice

Considering multiple known mechanisms of vascular leakage in acutely injured brain, we then examined effects of viral mimetic on BBB leakage of a small molecule and vessel architecture using vessel painting (VP) that utilizes perfusion of a small fluorescent lipophilic molecule DiI (~934 Da).²⁸ Confocal microscopy of the MCA territory at 24h revealed prominent extravasation of DiI in secondary and tertiary branches (Figure 2A), ranging from miniscule deposits to larger DiI “blooms”, some of which encompassed the vessel (Figure 2A, white arrows). Large DiI leakages were observed only in Poly-IC-treated mice, whereas foremost contributor to BBB leakages were vessels <100 μ m² (Figure 2B to D). Permutations of the small size vessels were most prominent at 24h and 72h after Poly-IC (white arrows), with a progressive temporal increase in small BBB leakages resulting in a ~3-fold increase at 10d. Poly-IC also triggered significantly increased lacunarity 10d after administration, particularly in males (Figure 2E and F). Altogether, these results suggest increased temporal structural and functional vulnerability of the vascular architecture after Poly-IC.

Poly-IC administration resulted in a global cortical decrease in vessel density over time (Figure 3A, B, and D), including a significant reduction at 24h with a trending decrease at 10d (Figure 3B). Vessel junction density was also significantly reduced by Poly-IC at 24h and 10d (Figure 3C). When mice were grouped

by sex, a significant reduction in vessel density was observed at 24h in males (Figure 3E). We also analyzed total vessel length and junction density in both males and females 24h, 72h, and 10 days after Poly-IC and PBS in both males and females. These results revealed that Poly-IC induced a significant decrease in junction density at 24h in males and at 10 days in female mice (Supplementary Figure 2A–B).

Confocal microscopy of the axial right MCA vascular territory (Figure 3F) revealed a significant decrease in vessel density 24h after Poly-IC (Figure 3G and H), where female mice contributed to the significant decrease in MCA vascular density at 24h (Figure 3H). Junction density in the MCAO vascular territory was not significantly altered in contrast to the whole right cortical hemisphere (Figure 3I). These findings demonstrate potential region-dependent effects of Poly-IC on the MCA vascular architecture and selected sex-dependence.

Poly-IC triggers sustained leukocyte recruitment to the cortex including early neutrophil infiltration and inflammatory cytokine response

Considering that Poly-IC could disrupt BBB integrity via several mechanisms, including modulating the immune response, we tested whether Poly-IC activates leukocytes and promotes their accumulation in brain parenchyma. Using flow cytometry (gating strategy in Figure 4A), we examined CD45^{high}CD11b⁺ myeloid cells (Figure 4B), CD45^{high}CD11b⁺Ly6c^{high} inflammatory monocytes (Figure 4C), CD45^{high}CD11b⁺Ly6c^{int}Ly6g⁺ neutrophils (Figure 4D) and CD45^{high}CD11b⁺Ly6c^{int}Ly6g⁽⁻⁾ patrolling monocytes (Figure 4E). Poly-IC significantly increased the levels of CD45^{high}CD11b⁺ myeloid cells in the cortex at 6h and the overall number remained similarly increased until 72h. Particularly, immune response was neutrophil-skewed early on.

Cytokine/chemokine profiling 3h after Poly-IC injection showed significantly increased levels of principle neutrophil chemoattractant, KC, and of monocyte/microglial chemoattractants MCP-1 and MIP-1 α , of IL-6, along with Eotaxin and G-CSF, which are involved in neutrophil maturation and signaling (Figure 4F), but essentially unchanged brain levels of TNF α and IL-1 β (Figure 4F).

To evaluate the involvement of the peripheral inflammatory component of Poly-IC administration and its impact on the blood-CSF barrier, we determined levels of same cytokines and chemokines in plasma and in the CSF. In plasma, the pattern of changes was similar to the one observed in the brain (Figure 4G), i.e., robust and significant increase of IL-6, Eotaxin and G-CSF and neutrophil and monocyte

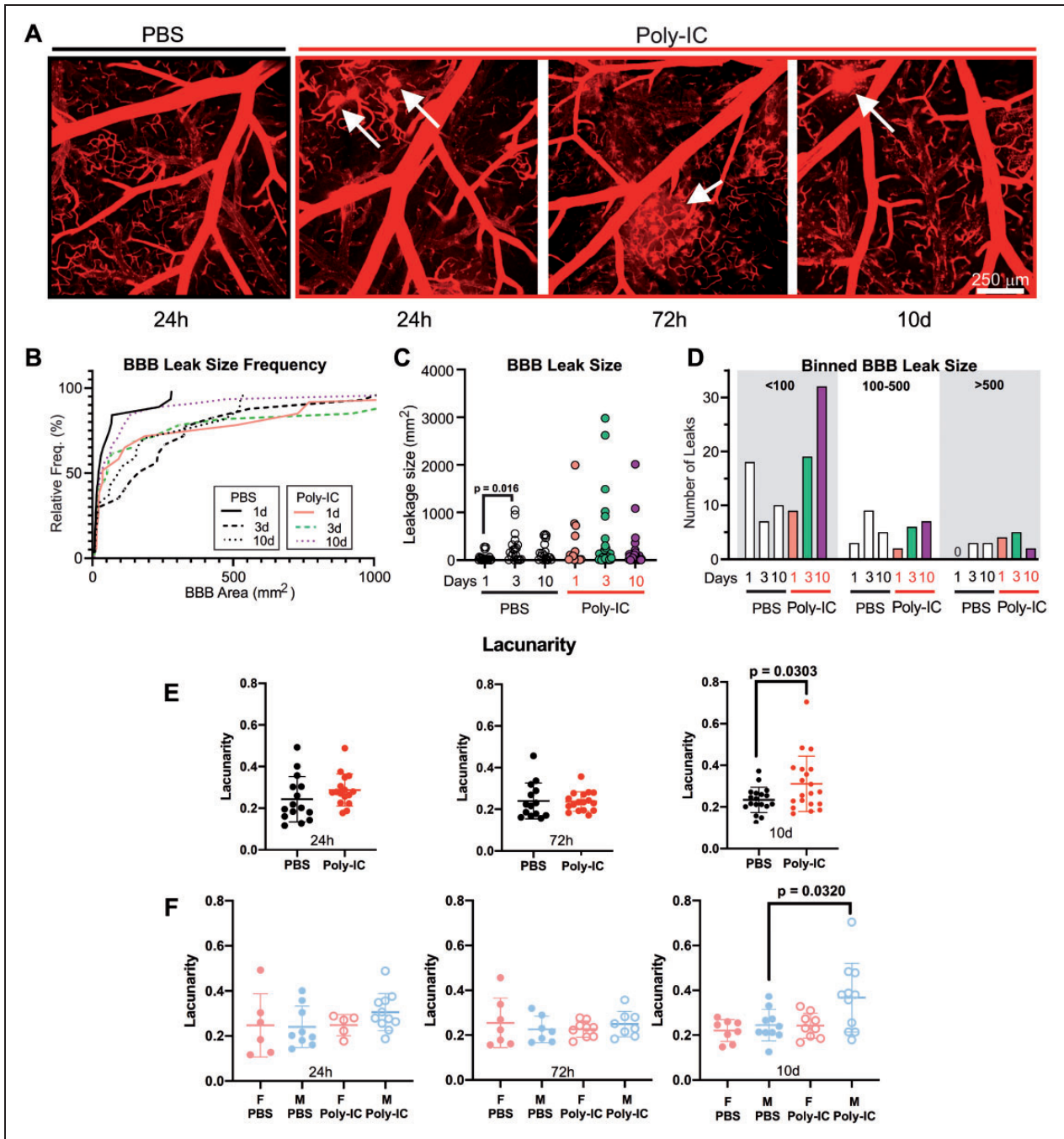


Figure 2. Poly-IC increases vascular leakage of a small molecular weight lipophilic molecule. (A) Confocal microscopy images of the VP using Dil within the MCA vascular territory in P18 mice treated with PBS or Poly-IC at 24h, 72h and 10d. White arrows denote BBB leakages. (B) A relative frequency histogram plot illustrates both the variation in size and frequency (at a particular size) of leakages within the MCA territory. Histogram is truncated at 1000 (see C). (C) The size of BBB leakages is plotted at each time point for PBS and Poly-IC treated mice. (D) Size distribution of BBB leakages assessed into 3 bins, <100, 100–500, and >500 mm², at 1, 3, and 10d after Poly-IC and PBS. Lacunarity at 24h, 72h and 10d following PBS or Poly-IC (E) and separated by sex (F). Two-way ANOVA with post-hoc Tukey’s Multiple Comparison test was performed to compare groups with multiple independent variables (C and F). Student’s t test with Mann-Whitney U test was performed to compare groups with non-normal distribution (E). Individual p values are listed within figures for data that are significant.

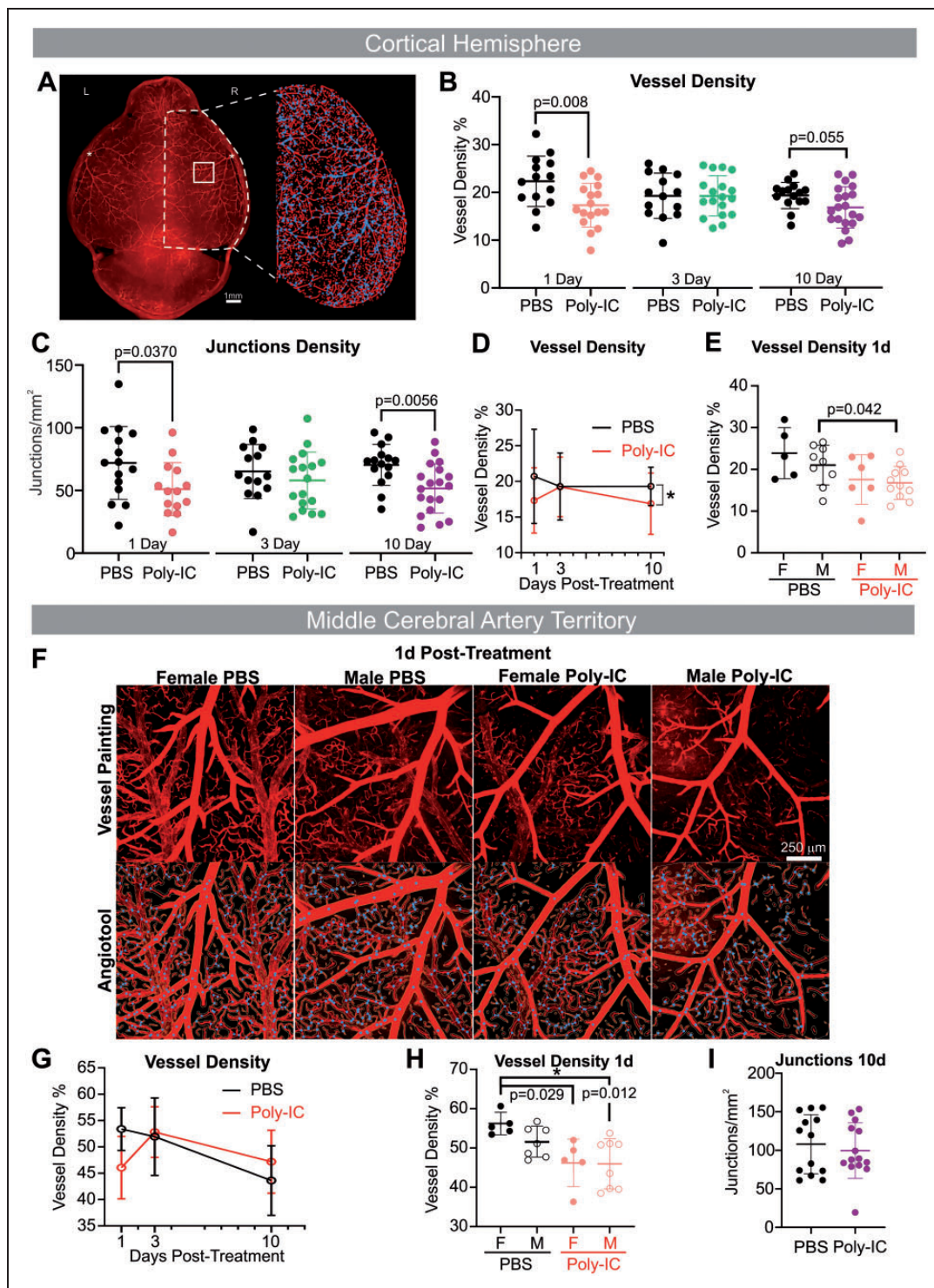


Figure 3. Poly-IC alters the developing vascular network. (A) An example of vessel painted brain from a male 1d post Poly-IC treatment. The vascular features for the right cortical hemisphere (RH) are expanded in the right panel illustrating the features utilized for analyses (blue = junctions, red = vessels). Cortical vessel density (B) and junction density (C) in PBS and Poly-IC mice 1, 3, and 10d after injection revealed early and late alterations. (D) Longitudinal vessel density in PBS and Poly-IC mice. E. Vessel density data separated by sex. F. Confocal images of the right middle cerebral artery (rMCA) illustrate reduced vascular features, such as vascular density at 1d after Poly-IC treatment in both sexes. The bottom panel shows the corresponding vascular analyses (blue = junctions, red = vessels). G-I. Temporal analyses of MCA vascular density in PBS and Poly-IC mice 24h, 72h, and 10d after injection and (H) separated by sex 1d after injection. I. Junctional density at 10d after PBS and Poly-IC. Two-way ANOVA with post-hoc Tukey's Multiple Comparison test was performed to compare groups with multiple independent variables (B, C, E, and H). Two-way ANOVA with Sidak post-hoc analysis was performed to compare treatment versus time and treatment versus sex (D and G). Student's t test with Mann-Whitney U test was performed to compare groups non-normal distribution (I). Individual p values are listed within figures for data that are significant.

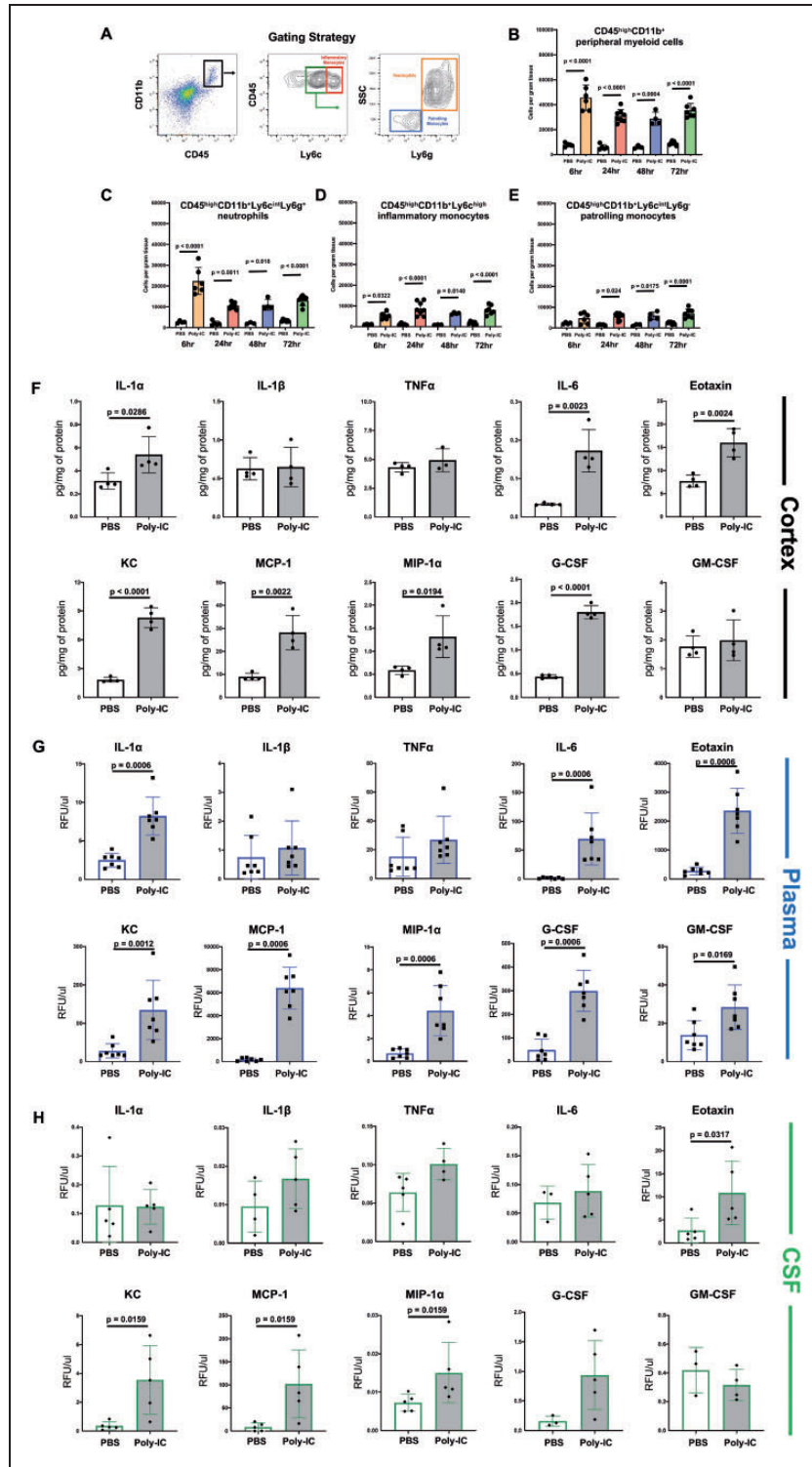


Figure 4. Poly-IC triggers sustained leukocyte recruitment to the cortex including early neutrophil infiltration and inflammatory cytokine response. (A) Gating strategy to identify leukocyte subpopulations. Quantification of individual leukocyte subtypes in the cortex 6h, 24h, 48h and 72h after PBS or Poly-IC administration. The relative number of CD45^{high}CD11b⁺ myeloid cells (B), CD45^{high}CD11b⁺Ly6c^{high} inflammatory monocytes (C), CD45^{high}CD11b⁺Ly6c^{int}Ly6g⁺ neutrophils (D) and CD45^{high}CD11b⁺Ly6c^{int}Ly6g⁻ patrolling monocytes (E). The levels of IL-1 α , IL-1 β , TNF α , IL-6, Eotaxin, KC, MCP-1, MIP-1 α , G-CSF and GM-CSF in the cortex (F), plasma (G) and CSF (H) 3h after PBS and Poly-IC. Two-way ANOVA with post-hoc Tukey's Multiple Comparison test was performed to compare groups with multiple independent variables (B–E). Student's t test with Mann-Whitney U test was performed to compare groups non-normal distribution (F–H). Individual p values are listed within figures for data that are significant.

chemoattractants KC, MCP-1, and MIP-1 α levels 3h after Poly-IC as compared to PBS (Figure 4G). Increased levels of inflammatory mediators in the blood neither triggered neutrophil accumulation in peripheral organs, liver and spleen, nor induced BSA leakage in these organs at 24h after Poly-IC (not shown). In the CSF, accumulation was also robust but was limited to increased levels of KC, MCP-1, and MIP-1 α (Figure 4H), consistent with rapid increase in neutrophil and monocyte number in the brains of Poly-IC treated mice (Figure 4B and C).

Cumulatively these data demonstrate the presence of both neuroinflammation and systemic inflammation and suggest a potential role for neutrophils in Poly-IC-triggered BBB disruption and may have roles in CSF-Brain interfaces as well.

Poly-IC promotes brain vascular associated neutrophils

To identify whether Poly-IC induces neutrophil vascular extravasation, we utilized immunofluorescence in WT and LysM-EGFP-ki mice. Occasional neutrophils were seen within the parenchyma of WT mice after Poly-IC injection, whereas the vast majority of Ly6G+ neutrophils were in close proximity and/or association with Glut-1+ vessels (Figure 5A and B). Co-labeling with Iba1 to differentiate neutrophils (Iba1-) and monocytes/macrophages (Iba1+) showed both cell types in the same vessel (Figure 5B). Neutrophils were also present in the choroid plexus (CP) 6h and 24h after Poly-IC (Supplementary Figure 3). Further, compared to PBS-treated LysM-EGFP-ki mice, 6h after Poly-IC the number of Ly6G+/GFP+ cells in CD31+ cerebral vasculature was increased in the cortex and striatum (Figure 5C to F), but remained low in the hippocampus (Figure 5F), meninges, CP and the ventricles.

Poly-IC rapidly induces neutrophil elastase (NE) and NETosis

Considering that neutrophils can induce vascular permeability via multiple mechanisms, we examined whether NE mediates Poly-IC-induced vascular distortions. Measurements of NE enzymatic activity in saline-perfused brains showed that compared to PBS, Poly-IC triggered a ~5-fold increase in NE activity within 6h in the cortex (Figure 5G), similarly in male and female mice (Supplementary Figure 4). NE activity gradually declined between 6h and 72h after Poly-IC but remained significantly elevated compared to PBS-treated mice (Figure 5G). Protein expression of NE and of citrullinated histone H3 (H3cit), a marker for

neutrophil extracellular trap formation (NETosis) and NE, were increased at 6h by Poly-IC (Figure 5H to J).

Double-immunofluorescence showed that Poly-IC upregulated NE in a subpopulation of Ly6G+ cells in saline perfused mice (Figure 5K to N) and that Ly6G+NE+ cells were predominantly seen within the vessels. Considering that macrophages can also produce NETs, we quantified percentage of NE double-labeled with Ly6G+ and Ly6G- cells. Over ~80% of NE+ cells were Ly6G+ (Figure 5O) and many of these NE+Ly6G+ cells were present in the brain 6 hours after Poly-IC as compared to PBS treatment (Figure 5P). Considering that both infiltrated neutrophils and neutrophils loosely adherent to the vessels can affect vascular permeability in stroke and brain trauma in the adult and hypoxia-ischemia in neonates, we further characterized spatial pattern of NETosis in neutrophils loosely attached to vessels by examining NETosis in non-perfused brains at the same time points. H3cit staining, indicative of NETosis, was evident in Ly6G+ neutrophils loosely adherent to the vessels at both 6h and 24h after Poly-IC administration (Figure 5Q). We also observed Ly6G+H3cit+ cells in the choroid plexus 6h and 24h after Poly-IC (Supplementary Figure 3A-B). Quantification of Ly6G+/GFP+ cells in LysM-EGFP-ki mice following PBS and Poly-IC injection in the meninges, CP and corpus callosum showed no statistically significant changes between groups in these regions (Supplementary Figure 3C). These data suggest that early NE activation and NETosis triggered in neutrophils infiltrated into the parenchyma and in loosely adherent cells promote vascular defects apparent at later time points (Figures 1 and 2).

Sivelestat attenuates vascular leakage in the cortex of Poly-IC-treated mice by reducing NE activity and changing the neuroinflammatory microenvironment

To establish causality for neutrophil-induced vascular disturbances, we used a potent NE inhibitor sivelestat (SIV; also known as ONO 5046; IC₅₀ = 44nM³⁰), an agent that showed promise in preclinical models of adult stroke^{31,32} and spinal cord injury.³¹⁻³³ Dosing regimen protocol was optimized in preliminary experiments to generate experimental design for SIV and vehicle (VEH) administration (Figure 6A). SIV significantly inhibited NE activation at 6h (Figure 6B) and 24h after Poly-IC compared to VEH treated mice. Effects of SIV were similar in males and females (Supplementary Figure 4).

SIV administration did not affect albumin^{Alexa-647} leakage in PBS-treated mice while it significantly attenuated leakage at 72h in VEH-treated compared to Poly-IC treated mice (Figure 6C and D). Moreover, SIV attenuated Poly-IC-induced upregulation of

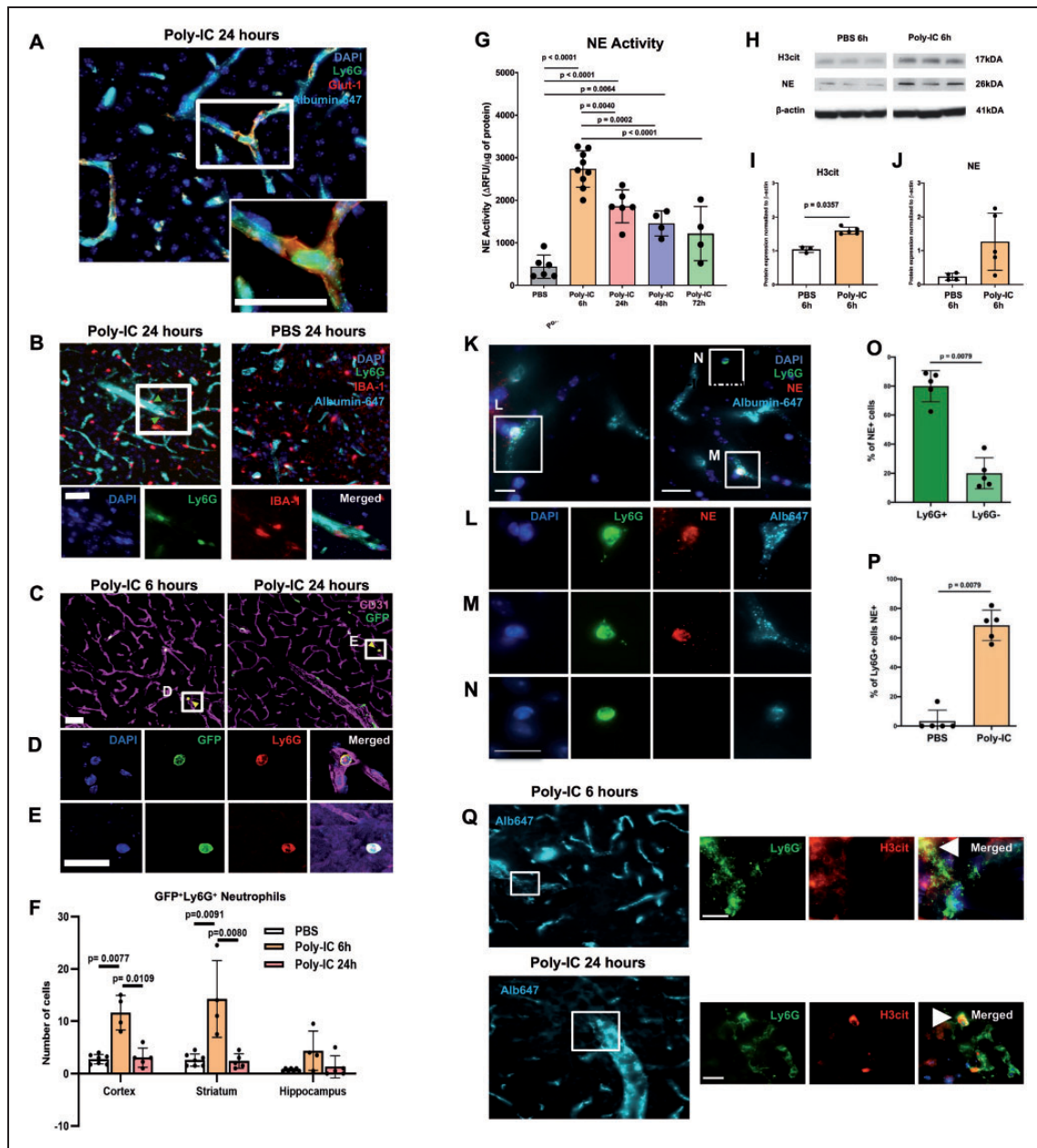


Figure 5. Poly-IC promotes brain vascular associated neutrophils and NET activity. (A-E) Spatial distribution of neutrophils in the brain following PBS and Poly-IC administration. (A and B) Ly6G⁺ neutrophils are present within vessels in the cortex of wild-type mice 24h after Poly-IC (A,B on the left) but not after PBS administration (B, on the right). Ly6G⁺ neutrophils associated with a vessel are shown in white box (B, left). Images in the bottom: higher magnification images of Ly6G⁺ neutrophils (green), vessel perfused with albumin^{Alexa-647} (cyan) and Iba1⁺ microglial/macrophages (red) from white box in b. (C-E) Representative images of EGFP+ EGFP+/Ly6G+ neutrophils 6h and 24h after Poly-IC and PBS administration in LysM-EGFP-ki mice. (D) and (E) indicate high magnification images in white boxes, with yellow arrows pointing to double positive GFP+/Ly6G+ neutrophils. (F) Quantification of double positive GFP+/Ly6G+ neutrophils in the cortex, striatum and hippocampus 6h and 24h after Poly-IC. Most Ly6G⁺ neutrophils are associated with vessels but are occasionally present in the parenchyma. Scale bar = 50 μ m. (G) Neutrophil elastase (NE) enzymatic activity in the cortex after PBS and 6-72h after Poly-IC administration. Data is shown as Δ RFU/ μ g protein. (H) Representative Western blots for H3cit, NE and β -actin. Quantification of H3cit (I), NE (J) relative to protein expression of β -actin 6h after PBS/Poly-IC administration. (K-N) Representative low magnification images of Ly6G⁺ neutrophils adjacent to subpopulation of vessels perfused with albumin^{Alexa-647} (K) (O) Quantification of neutrophil-associated (NE+/Ly6G+) and neutrophil independent (NE-/Ly6G-) NETosis 6h after Poly-IC in the cortex. (P) Quantification of % Ly6G⁺ cells that are NE+ 6h following PBS and Poly-IC administration. (Q) Higher magnification images of Ly6G+/NE+ cells demarcated in white boxes. Representative images of albumin^{Alexa-647} where high magnifications of Ly6G+/H3cit+ neutrophils in white box in non-perfused tissue taken 6h and 24h after Poly-IC in the cortex. Examples of Ly6G+/H3cit+ neutrophil identified with white arrows. Scale bars = 15 μ m. One-way ANOVA with post-hoc Bonferroni (normal distribution) or Kruskal-Wallis test (non-normal distribution) was performed to compare the variance in groups with one independent variable followed by Dunn post-hoc test (F and G). Student's t test with Mann-Whitney U test was performed to compare non-normally distributed data (I, J, O and P). Individual p values are listed in individual panels for data that are significant.

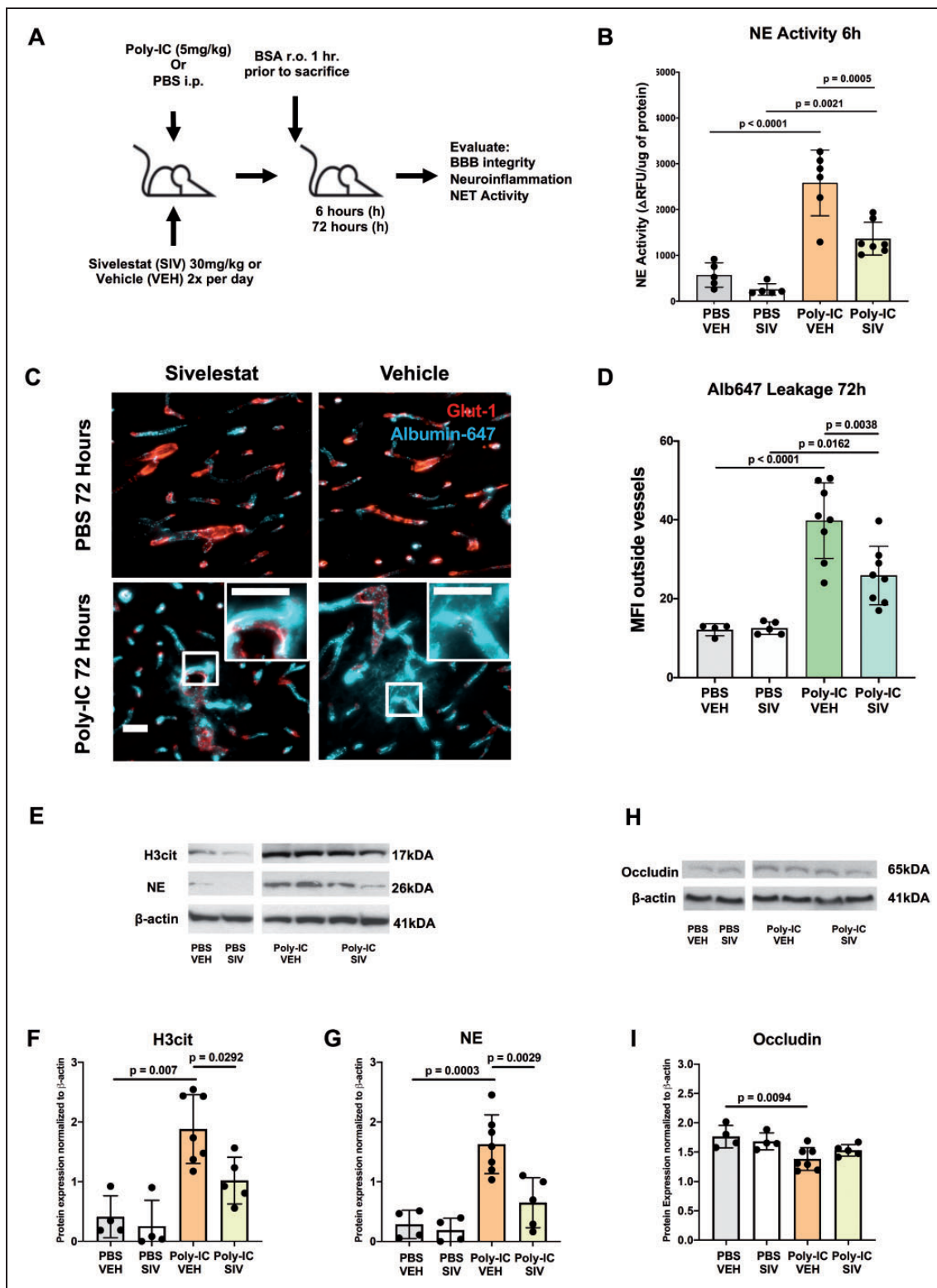


Figure 6. Sivelestat inhibits enzymatic activity of NE and reduces extravascular albumin leakage in Poly-IC treated mice. (A) Experimental design for VEH/SIV administration. (B) NE activity in the cortex 6h after PBS or Poly-IC administration, with/without VEH/SIV treatment. Data is shown as Δ RFU/ μ g protein. (C) Representative brain images following albumin^{Alexa-647} (i.v.; cyan) co-stained with GLUT-1+(red) 72h after PBS/Poly-IC with/without VEH/SIV treatment. (D) MFI of albumin^{Alexa-647} outside of vessels to quantify leakage in each group. Scale bar = 40 μ m. Representative Western blots for H3cit, NE (E) and occludin (H) 6h after PBS/Poly-IC administration with VEH/SIV treatment. Quantification of H3cit (F), NE (G), occludin (I) expression normalized to β -actin. Two-way ANOVA with post-hoc Tukey's Multiple Comparison test was performed to compare groups with multiple independent variables (B,D,F,G, and I). Individual p values are listed within figures for data that are significant.

NETosis-related proteins H3cit and NE (Figure 6E to G), but did not significantly affect occludin downregulation at 6h (Figure 6H and I).

Cytokine profiling at 6h revealed significant Poly-IC-induced accumulation of IL-1 α and IL-1 β , effects that were significantly diminished by SIV (Figure 7A). Interestingly, levels of IL-6, KC and MCP-1, which were elevated at 3h after Poly-IC (Figure 4F), remained unchanged at 6h, along with the levels of TNF α and G-CSF (Figure 7A). These data establish that NE activation and resultant NETosis mediate Poly-IC-induced vascular leakages in the brain of juvenile mice and that SIV administration can minimize the vascular effects through inhibition of NETosis and neuroinflammatory signaling.

Given that neutrophils were predominantly seen in association with vessels rather than infiltrated into the parenchyma, we examined expression of a main

receptor needed for neutrophil infiltration into the brain, CXCR2. Poly-IC significantly diminished the number of neutrophils expressing CXCR2 in the blood (Figure 7B) and CXCR2 expression remained unchanged in the cortex (Figure 7C), demonstrating that while neutrophils adhered to the cerebral vasculature in Poly-IC-treated mice, insufficient interaction between CXCR2 on peripheral neutrophils and KC in the brain, limited neutrophil abilities to infiltrate into the brain.

Discussion

In the first mouse model of viral infection-induced cerebral arteriopathy of childhood, we report a key role of the TLR3-neutrophil axis in disrupting the structure-functional integrity of neural vasculature and the developing vascular network, including Poly-IC triggered

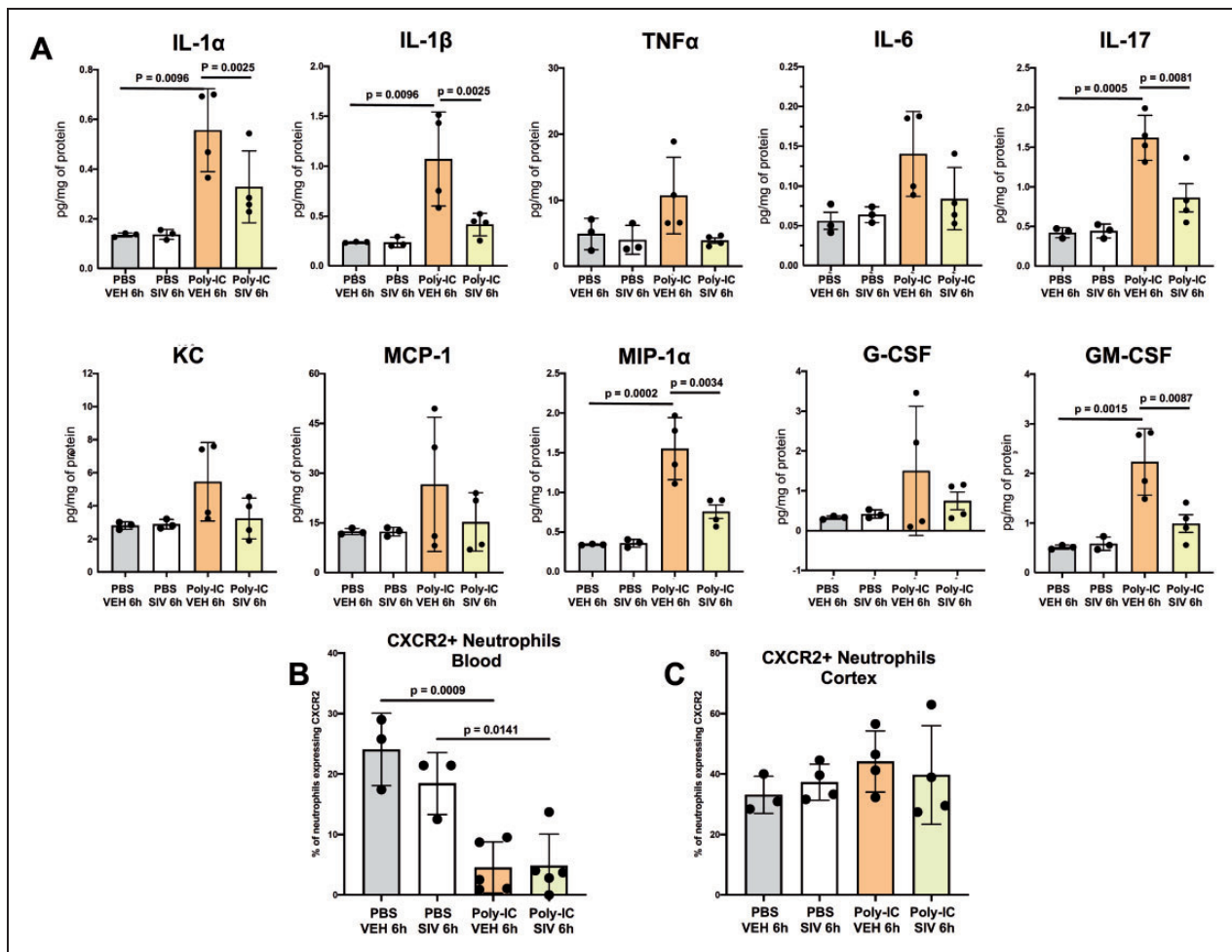


Figure 7. Sivelestat reduces cytokine expression in the cortex and reduces CXCR2+ expression in peripheral neutrophils 6h after Poly-IC administration. (A) The levels of IL-1 α , IL-1 β , TNF α , IL-6, IL-17, KC, MCP-1, MIP-1 α , G-CSF, and GM-CSF following PBS/Poly-IC and VEH/SIV treatment. Quantification of CXCR2⁺ neutrophils in blood (B) and cortex (C) 6h after PBS/Poly-IC administration with VEH/SIV treatment. Two-way ANOVA with post-hoc Tukey's Multiple Comparison test was performed to compare groups with multiple independent variables (A–C). Individual p values are listed within figures for data that are significant.

marked sustained extravascular albumin leakage, multiple changes at the BBB, rapid neutrophil-skewed immune response in the cerebral cortex and long-lasting disruption of the vascular architecture. Utilizing immunofluorescence, genetic, enzymatic and pharmacological approaches, we then demonstrate NE activation/NETosis as the novel underlying mechanism of vascular disturbances in juvenile mice induced by viral mimetic. Altogether, these data reveal a novel mechanism for viral-induced disruption of vascular integrity and vascular networks providing a potential therapeutic approach for preventing childhood arteriopathies and reducing susceptibility of the juvenile brain to consequences of CAIS.

International Pediatric Stroke Study demonstrated that cerebral arteriopathies are present in up to 80% of children with CAIS,² including focal cerebral arteriopathy of childhood,³⁴ and are strongly predictive of stroke recurrence.^{1,2,35} The Vascular Effects of Infection in Pediatric Stroke study further identified the presence of arteriopathy as the sole predictor of stroke recurrence.⁹ Imaging showed thickened neurovascular walls, inflammation and increased tortuosity of cerebral arteries, resulting in arterial stenosis and vascular irregularities.³⁶ Identification of inflammatory biomarkers in serum from children with arteriopathy further point to immune-mediated mechanisms of arteriopathies.³⁷ Viral infections, including varicella zoster virus (VZV), are major predictors of cerebral arteriopathy in children,¹ but infection-induced cerebral arteriopathy and the underlying mechanisms are unknown. We filled this knowledge gap using a novel age-appropriate mouse viral infection model showing how the neutrophil-neurovascular axis modulates cerebrovascular disturbances.

Poly-IC is a synthetic ligand for the innate immune receptor TLR3, receptor that recognizes double-stranded RNA (dsRNA) produced by viruses during replication³⁸ with varying context- and age-dependent effects *in vivo*. In the adult, TLR3 activation induces multiple inflammatory pathways³⁹ whereas TLR3 deficiency greatly reduces the inflammatory response to Poly-IC.³⁸ When administered just before or after cerebral ischemia, Poly-IC was shown to reduce injury via effects on astrocytes,⁴⁰ Fas/FADD interaction⁴¹ and stress response proteins Hsp27, Hsp70, and Bcl2.⁴² In contrast, in neonatal mice, Poly-IC sensitizes the brain to hypoxic-ischemic damage in a TLR3-mediated manner by initiating the inflammatory response.¹⁴ Here, leakage of albumin, small molecule DiI, and diminished expression of TJ proteins occludin and ZO-1 show a key role of Poly-IC/TLR3 signaling in functional BBB disturbances (i.e., leakage) in juvenile mice, including both transcellular and paracellular routes. Furthermore, effects of Poly-IC are not limited

to BBB leakage but induce vessel rigidity, as evident from thickened Col IV coverage, and rapid morphological distortions of the developing vascular architecture and vessel density, which remain prominent over days. While CBF was not tested in the Poly:IC group, the reduction in vessel density could implicate reduced ability of the vasculature to respond to adverse stimuli.

A dearth of literature exists concerning age-dependent vascular responses to inflammation. Neutrophils disrupt elastic lamina, leading to vasculopathy in both large and small vessels⁴³ but neonatal and adult neutrophils may behave differently in part because of variances in concentrations of microbicidal proteins, enzymes and cell surface receptors.⁴⁴ We reported preserved BBB integrity in acute neonatal stroke relative to that in adult stroke in part due to undeveloped smaller vessel/capillary network and dis-coordinated neutrophil ligand-CXCR2 receptor expression in neonates.²⁷ Increasing neutrophil chemoattractant gradient between the blood and the brain induced BBB leakage, led to neutrophil infiltration and amplified injury.²⁷ Injection of IL-1 β ⁴⁵ or rCINC-1 (KC in the mouse) into juvenile brain triggered profoundly higher neutrophil responses and vessel permeability in the brain, meninges, and CP compared to that in newborn or adult rats.^{45,46} Echoing preferential susceptibility of juvenile brain, we observed an enhanced neutrophil response in CAIS model⁶ compared to neonatal stroke model.⁵ In this study, we observed a peculiar systemic and cerebral cytokine/chemokine response to Poly-IC—an essential lack of early changes in IL-1 β and TNF α levels and transiently increased levels of neutrophil and monocyte chemoattractants (3h vs. 6h). Interestingly, we did demonstrate elevation of neutrophil and monocyte related chemoattractants Eotaxin, KC, MCP-1, and MIP-1 α in the CSF despite low levels of neutrophils in the CP, meninges and ventricles. Taken together, these results highlight profound age-specific effects of TLR3-mediated viral infection on the cerebral vessel architecture that may confer increased vascular vulnerability to CAIS.

In juvenile brains, Poly-IC rapidly induced significant accumulation of CD45^{high}/CD11b⁺/Ly6G⁺. Morphological analysis demonstrated increased number of neutrophils in vessels, but surprisingly, only modest infiltration of Ly6G⁺ cells in the brain parenchyma. Significantly diminished expression of KC's cognate receptor CXCR2 on peripheral neutrophils, in conjunction with only small and transient increases in brain KC levels early after Poly-IC, contributed to limiting infiltration of adherent neutrophils. Spatio-temporally, GFP+/Ly6G+ neutrophils and GFP+/Ly6G- or Iba1+/Ly6G- activated microglia/macrophages were often observed in proximity to the

same vessel, but there were no signs of morphological transformation of GFP+/Ly6G- or Iba1+/Ly6G- cells.

Neutrophils contribute to stroke via multiple mechanisms,^{43,47} but in the adult classic therapies targeting neutrophils have been largely ineffective.^{22,23} A growing number of studies are focusing on activation of NE, a serine protease that degrades the basal lamina and extracellular matrix.⁴⁸ NE is critical in host defense against microbial infection by mediating NETs released from activated neutrophils but disproportional activation of NE/NETosis contributes to both acute and chronic brain inflammation in models of adult stroke, spinal cord injury, and juvenile traumatic brain injury^{24,25,49} impairing revascularization and remodeling after brain damage.⁵⁰ NE elevation in patients infected with VZV, along with disrupted elastic lamina, suggest a role for NE in viral pathology.⁵¹ Interestingly, studies of NETosis have focused on LPS/TLR4 in the brain while TLR3-mediated effects are typically described for peripheral organs.^{25,52,53} In our study, NE inhibitor sivelestat significantly attenuated albumin leakage induced by Poly-IC, linking NE activation and NETosis to BBB leakage.

Our findings provide conceptual framework for further studies to understand the overall significance of infection-induced vascular disturbances in juvenile brain for long-term health, yet many questions are to be answered. NETs architecture is complex and dynamic and NETs discharge and degradation are multifactorial,⁵⁴ but the extent of dependence of these processes on age/maturation and the type of brain injury is unknown. Our data clearly demonstrate that effects of viral mimetic are not limited to changes in the neurovasculature, as evident from the presence of both neuroinflammation and accumulation of inflammatory cytokines in the circulation, but neurovascular and parenchymal changes may also depend on particular viral stimuli. The role of sex in infection-induced vascular distortions in children is another insufficiently understood aspect, which can be critically important knowing that boys are substantially more prone to CAIS than girls are. The mechanisms for why boys are more susceptible are still largely undefined. Based on studies in neonatal mice Poly-IC induces neuroinflammation, which was evident from higher NFκB levels and delayed IRF3 nuclear translocation in males relative to females.⁵⁵ *Staphylococcus epidermidis*, in turn, sensitized neonatal males to hypoxia-ischemia-mediated brain injury but not females despite similar accumulation of brain cytokine/chemokine levels.⁵⁶ To that end, we identified that Poly-IC induced changes in cerebral vessels (lacunarity 10 days after administration) in males yet we did not observe sex differences with regards to NE activity or albumin leakage. Further studies on sex differences in

both neonatal and juvenile models are crucial to identify whether sex-specific therapies are necessary.

In conclusion, in the first model for childhood arteriopathies in juvenile mice induced by viral infection, we established a key role of TLR3-neutrophil axis in disrupting structure-function of vascular networks and identified NE activation and NETosis as major underlying mechanisms. We propose that inhibition of NE and disruption of associated NETosis may become a vital target to overcome consequences of cerebral arteriopathy in children by preserving the viral-sensitized vasculature, minimizing brain vulnerability to future waves of inflammation, and potentially reducing the risk and severity of CAIS and its recurrence observed in children.^{9,37}

Funding

The author(s) disclosed receipt of the following financial support for the research, authorship, and/or publication of this article: The work was supported by RO1 NS44025 (ZV), RO1 NS76726 (ZV), RO1 NS103483 (ZV, CM, AO, CJE), VR-2017-01409 (CM), ALFGBG-722491 (CM), FO2019-0270 (CM), Åhlen Foundation (CM).

Acknowledgements

The authors thank Jessica Santhakumar, Amy Jung and Miral Abbas for contributing to cryostat sectioning of the brains.

Declaration of conflicting interests

The author(s) declared no potential conflicts of interest with respect to the research, authorship, and/or publication of this article.

Authors' contribution

AR – performed experiments, analyzed data, wrote and revised the manuscript;
 AJ – performed experiments, analyzed data, contributed to writing and editing the manuscript;
 TC – performed experiments, analyzed data, contributed to writing and editing the manuscript;
 JF – performed experiments, analyzed data, contributed to writing the manuscript;
 JS – performed experiments and data analysis, contributed to editing the text;
 MH – performed experiments and data analysis, contributed to editing the text;
 CJE – analyzed data, contributed editing the manuscript;
 CM – designed and oversaw subset of experiments, analyzed data, contributed to writing and revising the manuscript;
 AO – designed and oversaw subset of experiments, analyzed data, contributed to writing and revising the manuscript;
 ZV – designed and oversaw the study, analyzed data, wrote and revised the manuscript.

ORCID iD

Zinaida S Vexler  <https://orcid.org/0000-0002-6491-1562>

Supplemental material

Supplemental material for this article is available online.

References

- Amlie-Lefond C, Bernard TJ, Sebire G, et al. Predictors of cerebral arteriopathy in children with arterial ischemic stroke: results of the International Pediatric Stroke Study. *Circulation* 2009; 119: 1417–1423.
- Ganesan V, Prengler M, Wade A, et al. Clinical and radiological recurrence after childhood arterial ischemic stroke. *Circulation* 2006; 114: 2170–2177.
- Fullerton HJ, Stence N, Hills NK, et al. Focal cerebral arteriopathy of childhood: novel severity score and natural history. *Stroke* 2018; 49: 2590–2596.
- Hagberg H, Mallard C, Ferriero D, et al. The role of inflammation in perinatal brain injury. *Nat Rev Neurol* 2015; 11: 192–208. PMID: 25686754.
- Fernandez-Lopez D, Faustino J, Daneman R, et al. Blood-brain barrier permeability is increased after acute adult stroke but not neonatal stroke in the rat. *J Neurosci* 2012; 32: 9588–9600.
- Faustino J, Chip S, Derugin N, et al. CX3CR1-CCR2-dependent monocyte-microglial signaling modulates neurovascular leakage and acute injury in a mouse model of childhood stroke. *J Cereb Blood Flow Metabol* 2019; 39: 1919–1935.
- Rayasam A, Faustino J, Lecuyer M, et al. Neonatal stroke and TLR1/2 ligand recruit myeloid cells through the choroid plexus in a CX3CR1-CCR2- and context-specific manner. *J Neurosci* 2020; 40: 3849–3861.
- Kirton A and deVeber G. Paediatric stroke: pressing issues and promising directions. *Lancet Neurol* 2015; 14: 92–102.
- Fullerton HJ, Wintermark M, Hills NK, et al. Risk of recurrent arterial ischemic stroke in childhood: a prospective international study. *Stroke* 2016; 47: 53–59.
- Johnson RH, Kho DT, O'Carroll SJ, et al. The functional and inflammatory response of brain endothelial cells to toll-like receptor agonists. *Sci Rep* 2018; 8: 10102.
- Matsuzaki H, Mikami Y, Makita K, et al. Interleukin-17A and toll-like receptor 3 ligand poly(I:C) synergistically induced neutrophil chemoattractant production by bronchial epithelial cells. *PLoS One* 2015; 10: e0141746.
- Gan T, Yang Y, Hu F, et al. TLR3 regulated poly I:C-induced neutrophil extracellular traps and acute lung injury partly through p38 MAP kinase. *Front Microbiol* 2018; 9: 3174.
- Baghel MS, Singh B, Dhuriya YK, et al. Postnatal exposure to poly (I:C) impairs learning and memory through changes in synaptic plasticity gene expression in developing rat brain. *Neurobiol Learn Memory* 2018; 155: 379–389.
- Stridh L, Mottahedin A, Johansson ME, et al. Toll-like receptor-3 activation increases the vulnerability of the neonatal brain to hypoxia-ischemia. *J Neurosci* 2013; 33: 12041–12051.
- del Zoppo GJ, Schmid-Schonbein GW, Mori E, et al. Polymorphonuclear leukocytes occlude capillaries following middle cerebral artery occlusion and reperfusion in baboons. *Stroke* 1991; 22: 1276–1283.
- Lindsberg PJ, Siren AL, Feuerstein GZ, et al. Antagonism of neutrophil adherence in the deteriorating stroke model in rabbits. *J Neurosurg* 1995; 82: 269–277.
- Barone FC, Hillegass LM, Price WJ, et al. Polymorphonuclear leukocyte infiltration into cerebral focal ischemic tissue: myeloperoxidase activity assay and histologic verification. *J Neurosci Res* 1991; 29: 336–345.
- Yamasaki Y, Matsuo Y, Zagorski J, et al. New therapeutic possibility of blocking cytokine-induced neutrophil chemoattractant on transient ischemic brain damage in rats. *Brain Res* 1997; 759: 103–111.
- Gidday JM, Gasche YG, Copin JC, et al. Leukocyte-derived matrix metalloproteinase-9 mediates blood-brain barrier breakdown and is proinflammatory after transient focal cerebral ischemia. *Am J Physiol Heart Circ Physiol* 2005; 289: H558–H568.
- Akopov SE, Simonian NA and Grigorian GS. Dynamics of polymorphonuclear leukocyte accumulation in acute cerebral infarction and their correlation with brain tissue damage. *Stroke* 1996; 27: 1739–1743.
- Tang Y, Xu H, Du X, et al. Gene expression in blood changes rapidly in neutrophils and monocytes after ischemic stroke in humans: a microarray study. *J Cereb Blood Flow Metabol* 2006; 26: 1089–1102.
- Krams M, Lees KR, Hacke W, et al. Acute Stroke Therapy by Inhibition of Neutrophils (ASTIN): an adaptive dose-response study of UK-279,276 in acute ischemic stroke. *Stroke* 2003; 34: 2543–2548.
- Harlan JM and Winn RK. Leukocyte-endothelial interactions: clinical trials of anti-adhesion therapy. *Crit Care Med* 2002; 30: S214–S219.
- Schonrich G and Raftery MJ. Neutrophil extracellular traps go viral. *Front Immunol* 2016; 7: 366.
- Pena-Martinez C, Duran-Laforet V, Garcia-Culebras A, et al. Pharmacological modulation of neutrophil extracellular traps reverses thrombotic stroke tPA (tissue-type plasminogen activator) resistance. *Stroke* 2019; 50: 3228–3237.
- Percie du Sert N, Hurst V, Ahluwalia A, et al. The ARRIVE guidelines 2.0: updated guidelines for reporting animal research. *J Cereb Blood Flow Metabol* 2020; 40: 1769–1777.
- Fernandez-Lopez D, Faustino J, Klivanov AL, et al. Microglial cells prevent hemorrhage in neonatal focal arterial stroke. *J Neurosci* 2016; 36: 2881–2893.
- Salehi A, Jullienne A, Wendel KM, et al. A Novel Technique for Visualizing and Analyzing the Cerebral Vasculature in Rodents. *Transl Stroke Res* 2019; 10: 216–230.
- Aghaeepour N, Finak G, Flow CAPC, et al. Critical assessment of automated flow cytometry data analysis techniques. *Nat Methods* 2013; 10: 228–238.
- Feng L, Zhu W, Huang C and Li Y. Direct interaction of ONO-5046 with human neutrophil elastase through (1)H NMR and molecular docking. *Int J Biol Macromol* 2012; 51: 196–200.

31. Matayoshi H, Hirata T, Yamashita S, et al. Neutrophil elastase inhibitor attenuates hippocampal neuronal damage after transient forebrain ischemia in rats. *Brain Res* 2009; 1259: 98–106.
32. Stowe AM, Adair-Kirk TL, Gonzales ER, et al. Neutrophil elastase and neurovascular injury following focal stroke and reperfusion. *Neurobiol Dis* 2009; 35: 82–90.
33. Tonai T, Shiba K, Taketani Y, et al. A neutrophil elastase inhibitor (ONO-5046) reduces neurologic damage after spinal cord injury in rats. *J Neurochem* 2001; 78: 1064–1072.
34. Fearn ND and Mackay MT. Focal cerebral arteriopathy and childhood stroke. *Curr Opin Neurol* 2020; 33: 37–46.
35. Fullerton HJ, Wu YW, Sidney S, et al. Risk of recurrent childhood arterial ischemic stroke in a population-based cohort: the importance of cerebrovascular imaging. *Pediatrics* 2007; 119: 495–501.
36. Lanthier S, Armstrong D, Domi T, et al. Post-varicella arteriopathy of childhood: natural history of vascular stenosis. *Neurology* 2005; 64: 660–663.
37. Fullerton HJ, deVeber GA, Hills NK, et al. Inflammatory biomarkers in childhood arterial ischemic stroke: correlates of stroke cause and recurrence. *Stroke* 2016; 47: 2221–2228.
38. Alexopoulou L, Holt AC, Medzhitov R, et al. Recognition of double-stranded RNA and activation of NF-kappaB by toll-like receptor 3. *Nature* 2001; 413: 732–738.
39. Field R, Campion S, Warren C, et al. Systemic challenge with the TLR3 agonist poly I:C induces amplified IFNalpha/beta and IL-1beta responses in the diseased brain and exacerbates chronic neurodegeneration. *Brain Behav Immun* 2010; 24: 996–1007.
40. Li Y, Xu XL, Zhao D, et al. TLR3 ligand poly IC attenuates reactive astrogliosis and improves recovery of rats after focal cerebral ischemia. *CNS Neurosci Therapeut* 2015; 21: 905–913.
41. Zhang X, Ha T, Lu C, et al. Poly (I:C) therapy decreases cerebral ischaemia/reperfusion injury via TLR3-mediated prevention of Fas/FADD interaction. *J Cell Mol Med* 2015; 19: 555–565.
42. Wang PF, Fang H, Chen J, et al. Polyinosinic-polycytidylic acid has therapeutic effects against cerebral ischemia/reperfusion injury through the downregulation of TLR4 signaling via TLR3. *J Immunol* 2014; 192: 4783–4794.
43. Aronowski J and Roy-O'Reilly MA. Neutrophils, the felons of the brain. *Stroke* 2019; 50: e42–e43.
44. Lawrence SM, Corriden R and Nizet V. Age-appropriate functions and dysfunctions of the neonatal neutrophil. *Front Pediatr* 2017; 5: 23.
45. Anthony DC, Bolton SJ, Fearn S, et al. Age-related effects of interleukin-1 beta on polymorphonuclear neutrophil-dependent increases in blood-brain barrier permeability in rats. *Brain* 1997; 120: 435–444.
46. Anthony D, Dempster R, Fearn S, et al. CXC chemokines generate age-related increases in neutrophil-mediated brain inflammation and blood-brain barrier breakdown. *Curr Biol* 1998; 8: 923–926.
47. Enzmann G, Mysiorek C, Gorina R, et al. The neurovascular unit as a selective barrier to polymorphonuclear granulocyte (PMN) infiltration into the brain after ischemic injury. *Acta Neuropathol* 2013; 125: 395–412.
48. Jickling GC, Liu D, Ander BP, et al. Targeting neutrophils in ischemic stroke: translational insights from experimental studies. *J Cereb Blood Flow Metabol* 2015; 35: 888–901.
49. Semple BD, Trivedi A, Gimlin K, et al. Neutrophil elastase mediates acute pathogenesis and is a determinant of long-term behavioral recovery after traumatic injury to the immature brain. *Neurobiol Dis* 2015; 74: 263–280.
50. Kang L, Yu H, Yang X, et al. Neutrophil extracellular traps released by neutrophils impair revascularization and vascular remodeling after stroke. *Nat Commun* 2020; 11: 2488.
51. Sun G, Ota C, Kitaoka S, et al. Elevated serum levels of neutrophil elastase in patients with influenza virus-associated encephalopathy. *J Neurol Sci* 2015; 349: 190–195.
52. Clark SR, Ma AC, Tavener SA, et al. Platelet TLR4 activates neutrophil extracellular traps to ensnare bacteria in septic blood. *Nat Med* 2007; 13: 463–469.
53. Kim SW, Lee H, Lee HK, et al. Neutrophil extracellular trap induced by HMGB1 exacerbates damages in the ischemic brain. *Acta Neuropathol Commun* 2019; 7: 94.
54. Adrover JM, Aroca-Crevillen A, Crainiciuc G, et al. Programmed ‘disarming’ of the neutrophil proteome reduces the magnitude of inflammation. *Nat Immun* 2020; 21: 135–144.
55. Chavez-Valdez R, Mottahedin A, Stridh L, et al. Evidence for sexual dimorphism in the response to TLR3 activation in the developing neonatal mouse brain: a pilot study. *Front Physiol* 2019; 10: 306.
56. Gravina G, Svedin P, Ardalan M, et al. Staphylococcus epidermidis sensitizes perinatal hypoxic-ischemic brain injury in male but not female mice. *Front Immunol* 2020; 11: 516."